Simulations numériques du comportement au jeune âge des structures en béton : Modélisation et retour d'expérience

Jean Louis Tailhan, Laetitia d'Aloia, Philippe Autuori

HAL Id: hal-00612155

https://hal.science/hal-00612155

Submitted on 28 Jul 2011

Numerical simulations of the early-age behavior of concrete structures: Modeling and feedback

Jean-Louis TAILHAN*
*Laboratoire central des Ponts et Chaussées,
Paris, France*

Laetitia D'ALOIA
*Centre d'Études des Tunnels,
Bron, France*

Philippe AUTUORI
*Bouygues Travaux-Publics,
Saint-Quentin-en-Yvelines, France*

■ ABSTRACT

An effective control over early-age behavior in concrete serves to guarantee successful applications on civil engineering project sites. Numerical tools designed to assist decision-making during the critical phases of concrete structure design and execution are indeed available. This document provides a summary presentation of a simple numerical simulation model of the thermomechanical behavior of early-age concrete; it offers insight into both the temperature and stress fields that develop as of the first few hours of concreting within structures and moreover enables conducting a cracking risk analysis. An industrial application example using this tool is also proposed herein.

Simulations numériques du comportement au jeune âge des structures en béton : modélisation et retour d'expérience
■ RÉSUMÉ

Une bonne maîtrise du comportement au jeune âge des bétons est l'assurance de garantir le succès de la réalisation d'un chantier de Génie Civil. Des outils numériques d'aide à la prise de décision dans les phases cruciales de la conception et de la réalisation des structures en béton existent. Ce document est une succincte présentation d'un modèle simple de simulation numérique du comportement thermomécanique du béton au jeune âge. Il donne accès aux champs de température et de contraintes qui se développent dès les premières heures de bétonnage dans les structures et permet de procéder à une analyse des risques de fissuration. Un exemple d'utilisation industrielle de cet outil est proposé.

***Corresponding author**:

Jean-Louis TAILHAN
jean-louis.tailhan@lcpc.fr

INTRODUCTION

Controlling the time required to complete a construction job is a critical parameter for contractors and civil engineering companies. Without delving into the details of all factors involved in this time management process, it often becomes relevant to answer the following question: how can formwork be removed as quickly as possible on the cast concrete elements while ensuring satisfactory execution quality? The prospect of rapid formwork removal leads to questioning whether the component material of the structural element being built has reached a sufficient state of maturity to perform its mechanical function, at least during the construction phase. Yet such an inquiry also entails verifying that fabrication conditions for project components do not lead to an eventual risk of cracking, which could jeopardize either the mechanical performance of these components or, over the longer term, lower their durability. This discussion refers heavily to a recurrent and key issue, namely the early-age behavior of concrete. Effective control of this behavior ensures the success of industrial production processes by facilitating decision-making during the pivotal phases of concrete structural design (choice of materials, placement of secondary reinforcement, choice of curing protocol, etc.) and execution (form panel rotation, prestressing steps, etc.).

An appropriate estimation of the mechanical behavior of early-age concrete requires an accurate description of the various physical mechanisms influencing this "life period" of the material. Incorporating such a description into the modeling tool, e.g. CESAR-LCPC [1, 2], makes this estimation step feasible. The joint application of a maturity meter or gauge and the experimental determination of material strength values enables conducting preliminary structural studies and optimizing the choice of: concrete mix design, concreting phasing, and introduction of ancillary treatments such as heat curing.

As a first step, the pertinent physical mechanisms will be reviewed and details provided regarding thermomechanical behavior modeling. The subsequent discussion focuses on the various resources available to determine the input dataset specific to thermal behavior modeling. The final section will present a case study in the use of these tools.

REVIEW OF THE PHYSICAL MECHANISMS INVOLVED

Cement hydration is manifested by a series of complex chemical reactions that, on the whole, display a highly exothermic nature. Moreover, these reactions are activated thermally, meaning that their kinetics become faster as temperature rises. The exothermic nature of these reactions leads to internal heat production, which generates a material temperature increase. Just a few hours after concrete pouring, temperatures can reach high levels (above 50°C at the core for massive structures). Later on, as reaction speed decreases and given the exchange conditions relative to the ambient atmosphere, the material temperature also drops. Not only does the concrete structure undergo temperature fluctuations over time, but at any given moment this temperature might not necessarily be uniform and therefore display nonzero internal gradients. Temperature evolution over time induces structural deformations (said to be of thermal origin), which once again are not necessarily homogeneous within the structure at any given time.

In conjunction with this finding, another phenomenon occurs during cement hydration. At the microscopic scale, chemical reactions incite the formation of hydrates. Le Chatelier noted (in [3]) that the volume of hydrates formed remained less than the sum of consumed water plus hydrated cement volumes. Following setting, this contraction is reflected by capillary shrinkage due to the creation of water meniscuses inside the hydrate pores. This particular phenomenon constitutes what is referred to as endogenous shrinkage.

Concrete is a material whose mechanical properties evolve over time as well [4]. If the deformations mentioned above (i.e. mainly thermal shrinkage during the cooling phase and endogenous shrinkage) are mechanically inhibited due to mechanical boundary conditions or bonding conditions between structural elements, then these deformations lead to stress levels capable of quickly reaching values in excess of the material's tensile strength at the studied age, in which case the material cracks.

BASIC MODELING PRINCIPLES

Our intention here is limited to recalling the modeling principles inherent in the TEXO and MEXO modules used in the CESAR-LCPC finite element computation code [1, 2]. Detailed bibliographies as well as a general modeling framework of early-age thermomechanical behavior based on a thermodynamic description of irreversible processes in porous media are available in [5-7] or [8].

The heat budget applied to a concrete volume element can be expressed by a standard heat equation that includes a source term to represent the internal heat production subsequent to exothermic chemical reactions, i.e.:

$$C\frac{\mathrm{d}T}{\mathrm{d}t} = -div(\mathbf{q}) + Q_{\infty}\frac{\mathrm{d}r}{\mathrm{d}t} \tag{1}$$

where C denotes the volumetric heat capacity, $\mathbf{q}$ the heat flux density, Q_{∞} the total heat released by cement hydration (assumed to be constant and determined from a calorimetric test, *see* previous section).

The volumetric heat capacity, C, is a function of a number of parameters, primarily the degree of hydration and temperature. Depending on the degree of hydration, variations in C are evidenced by a decrease in this parameter's value. Yet on the other hand, temperature rise triggers an increase in C, which offsets the drop indicated above. It is thus customary to consider C as being constant [9].

The vector $\mathbf{q}$ is classically given by a Fourier Law, of the form:

$$\mathbf{q} = -\mathbf{K} \cdot \mathrm{grad}\,T \tag{2}$$

where (with $\mathbf{I}$ being the identity matrix) $\mathbf{K} = k\mathbf{I}$ represents the material conductivity, which is most often assumed to be isotropic. Many parameters are capable of influencing the conductivity value, including: water content of the concrete, type of aggregate, porosity, temperature, and degree of reaction progress [8]. According to the standard approach however, these parameters are assumed to cause only minute variations in k, making it feasible to consider conductivity as a constant as well. In contrast, it may be relevant to incorporate, through a homogenization method for example, the quantity of reinforcement present in the concrete since reinforcement can exert a significant impact on heat transfer.

The thermal exchange conditions at the boundaries are expressed by:

$$\mathbf{q} \cdot \mathbf{n} = \lambda \, (T - T_{\mathrm{imp}}) \tag{3}$$

where λ is the exchange coefficient and T_{imp} the outside temperature.

In Equation (1), r denotes the level of reaction progress. The quantity of heat released, at time t, by means of the hydration reaction is then given by:

$$Q(t) = r(t)\, Q_\infty \quad \text{with} \quad 0 \leq r(t) \leq 1 \tag{4}$$

It is straightforward to prove that based on Equation (1) and under adiabatic conditions, $Q(t) = C(T^{\mathrm{ad}}(t) - T_0)$, which yields an expression for the level of reaction progress as a function of a ratio of adiabatic temperatures:

$$r(t) = \frac{Q(t)}{Q_\infty} = \frac{T^{\mathrm{ad}}(t) - T_0}{T^{\mathrm{ad}}_\infty - T_0} \tag{5}$$

This level of reaction progress reveals the degree of cement hydration, ξ. By definition [6], the degree of cement hydration is the ratio of the mass of water consumed at time t by the hydration reaction to the mass of water required for complete cement hydration (equal to approx. 20% of the cement quantity used in the mix). Consequently, the degree of hydration never equals 1 since cement grain hydration always remains incomplete. Let's call ξ_∞ the final degree of hydration, then r can be correlated with ξ by the following expression:

$$\frac{\xi}{\xi_\infty} = \frac{r}{r_\infty} = r \quad \text{car} \quad r_\infty = 1 \tag{6}$$

These equations are complemented by a macroscopic description of hydration kinetics; the kinetic law employed (in accounting for the thermoactive characteristic of reactions) is of the following form:

$$\frac{\mathrm{d}r}{\mathrm{d}t} = \tilde{A}(r) \exp(-\frac{E_{\mathrm{a}}}{RT}) \tag{7}$$

where $\dfrac{E_{\mathrm{a}}}{R}$ represents the Arrhenius constant and $\tilde{A}$ the standardized affinity, which depends solely on the degree of hydration, thus implying that it also depends on the level of progress r and the concrete composition.

The source term is therefore known once all necessary experimental data have been collected relative to:

– the total quantity of heat potentially released by the material, a value that typically depends, among other things, on clinker composition, cement additives and concrete composition. With knowledge of this quantity, the value of Q_∞ can then be deduced;

– hydration kinetics, i.e. the data used to estimate standardized affinity $\tilde{A}(r)$;

– activation energy E_a, which allows calculating Arrhenius' constant $\dfrac{E_a}{R}$

These data are typically derived from the kinds of experiments described below.

It was previously mentioned that while the hydration reaction can be reflected at the microscopic level by an increase in the quantity of hydrates, at the macroscopic level it leads to: a change in material stiffness, endogenous shrinkage due to self-desiccation (resulting from Le Chatelier's contraction), and heat-induced strains.

From a mechanical perspective, in considering the material's elasticity and neglecting creep effects, these properties give rise to the following stress expression:

$$\mathrm{d}\sigma = \left(K(r) - \frac{2}{3}G(r) \right)\mathrm{d}\varepsilon\ \mathbf{I} + 2G(r)\ \mathrm{de} - 3\alpha k\ \mathrm{d}T\ \mathbf{I} + 3\varepsilon_f\ \mathrm{d}r\ \mathbf{I} \tag{8}$$

$K(r)$ and $G(r)$ are respectively the modulus of compressibility and shear modulus, α is the coefficient of thermal expansion and ε_f the final endogenous shrinkage.

The modulus of compressibility and the shear modulus, which are easily correlated with both Young's modulus and Poisson's ratio by means of the following relationships, depend on the degree of hydration, hence on the r value, of the material [4].

$$K(r) = \frac{E(r)}{3(1-2\mathrm{v})} \quad \text{and} \ \ G(r) = \frac{E(r)}{2(1+\mathrm{v})} \tag{9a and 9b}$$

Poisson's ratio is assumed to be constant, given the relative paucity of results in the literature and the fact that the bulk of its evolution occurs at low degrees of hydration [9]. The evolution in modulus of elasticity is given by an adaptation of Byfors' Law:

$$E(r) = E_\infty f(r) \tag{10}$$

with:

$$f(r) = \frac{1 + 1,37 R_{c\infty}{}^{2,204}}{1 + 1,37 R_c(r)^{2,204}} \left[\frac{R_{c\infty}}{R_c(r)} \right]^{2,675} \quad \text{and} \ \ R_{c\infty} = \left[\frac{E_\infty}{7250} \right]^{\frac{1}{0,471}} \tag{11a and 11b}$$

where E_∞ and $R_{c\infty}$ denote respectively the Young's modulus and compressive strength of the hardened material. Moreover, $R_c(r)$, which represents compressive strength, is expressed by the bilinear function of r (with r_0 being the material's mechanical percolation threshold):

$$R_c(r) = \begin{cases} rR_{co} & \text{si} \quad r \leq r_0 \quad \text{avec} \quad R_{co} = r_0 R_{c\infty}/10 \\[2mm] (R_{c\infty} - R_{co})\dfrac{r - r_0}{1 - r_0} + R_{co} & \text{si} \quad r > r_0 \end{cases} \tag{12a and 12b}$$

It can also be noted that in the behavior law shown in (8), the coefficients of thermal expansion α and chemical shrinkage ε_f are, as an initial approximation, assumed constant. More specifically, the strain due to chemical shrinkage is assumed to vary linearly with respect to the degree of hydration, thus with respect to r. This relationship leads to a slight overestimation at lower r values. (For additional details, the interested reader is directed to the literature on the variations in these two parameters relative to the degree of hydration: see bibliographic reference [9].)

In practical terms, thermomechanical coupling has been taken into account to a very little extent: the mechanical computation (in the MEXO module), which requires knowing temperature evolution within the structure, is conducted subsequent to the thermal computation (TEXO). The latter result provides a temperature field estimation at each computation time step, with this output then being used by MEXO to estimate the stresses stemming from heat-induced strains. The underlying hypothesis adopted for this weak coupling assumes that the material's (purely mechanical) strain effect on thermal behavior remains negligible.

EXPERIMENTAL CHARACTERIZATION OF CONCRETE HEAT RELEASE

■ Experimental set-up

Two main types of experimental devices are available to perform heat release tests, for the purpose of characterizing the heat release characteristics of a concrete specimen:

QAB (quasi-adiabatic) caissons: heat release testing under semi-adiabatic conditions on concrete (cylindrical specimens 16 cm in diameter and 32 cm high, for a total volume of approx. 6.5 liters) **[10]**.

Adiabatic calorimeters (of the CERILH type): heat release testing campaign under adiabatic conditions on a concrete specimen with 2.5 liters equivalent of concrete) **[11]**.

Semi-adiabatic conditions relate to partial exchanges with the ambient medium and, as such, require calculating heat losses. To proceed under these conditions, the atmosphere must be fully regulated and the various calorimeters calibrated (*see* **[13]**). Moreover, a calorimeter containing an inert (already hardened) sample is used as an atmospheric control and accounts for the effects of calorimeter inertia (temperature variations do not exert an immediate impact on the test sample).

Adiabatic conditions indicate partial exchanges with the ambient medium; these conditions are obtained by setting, throughout the test period, the temperature of the heating chamber containing the sample equal to the sample temperature. A lack of temperature differential between the sample and its immediate environment serves to eliminate all heat exchanges. A cryostat has also been set at 10°C to regulate the outer shell temperature of the calorimeter containing both the sample and the heating chamber. This shell allows conducting tests at below ambient temperature.

Remark: In addition to laboratory measurements, it may be foreseen to measure temperature on massive specimens; these recordings would offer an improved calibration of material parameters, as determined in the laboratory, and the possibility to incorporate laboratory/worksite variations. Such additional measurements would provide a better calibration of *in situ* heat exchange coefficients and, as a result, introduce more realistic boundary conditions.

■ Heat release calculation

Heat release is calculated from temperature measurements. For each test conducted, an increase in the temperature of both sample and calorimeter is observed, thus requiring the heat capacity of the calorimeter in use, since the heat capacity of concrete is calculated based on its mix design as well as on the heat capacities of material components. Three calibration coefficients for the semi-adiabatic calorimeters are derived (two heat exchange coefficients, and heat capacity of the empty calorimeter), plus one calibration coefficient for the adiabatic calorimeter (just the heat capacity when empty).

Practically speaking, each point in time is associated with a temperature measurement $T(t)$, including the control device temperature $T_t(t)$, from which the quantity of heat released $Q(t)$ can be deduced (in most instances correlated with the quantity of cement m_c contained in the sample, denoted $q(t) = \dfrac{Q(t)}{m_c}$. This calculation is performed by considering the fact that a portion of the energy is stored in the form of heat, while the other portion is ultimately dissipated towards the ambient medium, $P(t)$.

› Case of semi-adiabatic testing

$$q(t) = \frac{C}{m_c}\big(\theta(t) - \theta_0\big) + P(t) = \frac{C}{m_c}\big(\theta(t) - \theta_0\big) + \frac{1}{m_c}\int_0^t \big(a\theta(\tau) + b\theta^2(\tau)\big)\,\mathrm{d}\tau \qquad \textbf{(13)}$$

with:

C: total heat capacity (for the sample, mold and empty calorimeter),

$\theta(t) = T(t) - T_t(t), \theta_0$: heating of the sample at time t and initial heating,

a, b: heat loss coefficients of the calorimeter.

› Case of adiabatic testing

In the special case of adiabatic tests, heat loss vanishes, i.e. $P(t) = 0$, and the expression of heat release can be simplified as:

$$q(t) = \frac{C}{m_c}\left(T(t) - T_0\right) \tag{14}$$

with:

T_0: initial sample temperature.

■ Analysis of heat release results and determination of E_a

A calorimetric test offers a characterization of the heat lost from a concrete specimen, i.e. heat release (or hydration) kinetics and total quantity of heat released Q_∞.

In the case of semi-adiabatic tests, the heat release curve obtained is correlated with a given temperature history, whereas in the case of adiabatic tests, the heat release curve is intended to be correlated with a specific temperature history, to the extent that self-curing is complete: all the heat released goes towards raising sample temperature. This temperature curve can also be called, for example, the 20°C adiabatic curve.

The parameter that enables, in theory, bridging test results or predicting heat release under a given set of conditions (as is the case with numerical simulations) would be the apparent activation energy of concrete, E_a. This parameter characterizes the sensitivity of heat release kinetics for a given concrete mix design to temperature variation and stems from Arrhenius' Law applied to cement hydration **(Equation 7)**.

Accordingly, a comparison of two tests (whether adiabatic or semi-adiabatic) at two distinct initial temperatures, in generating two distinct thermal histories, leads to calculating this activation energy E_a.

In practice, it needs to be pointed out that the TEXO module can only accommodate a strictly increasing adiabatic curve (either directly input or deduced by software from semi-adiabatic results). This condition however does not always replicate the reality of calorimetric testing. Uncertainties related to temperature measurements and heat loss coefficient calibration, or alternatively heat capacity of the empty calorimeter, yield corrected temperature or heat curves that sometimes slope downward ever so slightly at the end of the test rather than tending towards a threshold considered to correspond with the final heat release value. If the magnitude of this downward trend remains insignificant, then the test is validated but still cannot be input as is into the TEXO module.

Furthermore, it is critical to include, as TEXO input, a temperature trend curve corresponding to nearly all of the heat released, in order for the thermal and mechanical simulations to convey real meaning. The degree of concrete hydration progress ranges from 0 to 1 and is calculated on the basis of heat released, as revealed by the quasi-adiabatic or adiabatic test results. The evolution in mechanical characteristics can then be evaluated using r; if the test results inputted into TEXO are only partial, then both thermal and mechanical calculation results would be erroneous.

INPUT OF DATA SPECIFIC TO THE TEXO MODULE AND BOUNDARIES

These data, used to characterize the heat release of a concrete specimen, are input in the following form:

A series of triplets, composed of time, concrete temperature and control temperature (or initial concrete temperature in the case of an adiabatic test), retracing the thermal history of the concrete specimen throughout the heat release test. This curve is associated with both the calorimeter's heat loss coefficients (equal to zero in an adiabatic test) and total heat capacity.

The apparent activation energy of concrete can be preliminarily determined from two tests undertaken at two distinct temperatures.

The first data element provides information on kinetics $\tilde{A}(r)$ and total quantity of heat released, whereas the second serves to characterize the sensitivity of concrete to a temperature variation.

The validity range of simulations based on a determination of these two data needs to be specified. As regards the heat release curve, it may be considered that only those simulations run for initial concrete temperatures close to the test temperature are indeed satisfactory. Generally speaking, the test is conducted for a 20°C initial temperature, while the initial temperatures of concrete specimens being simulated lie between 5 and 35°C. The same would apply to activation energy; moreover, it is typically recommended to select the type of test (i.e. adiabatic vs. semi-adiabatic) based on the given application (massive structure vs. thin structure).

MATURITY READINGS IN ASSOCIATION WITH NUMERICAL TOOLS

"Maturity measurements" or "Equivalent age method" incorporates the coupled effects of temperature and time in predicting compressive strength during the early age of concrete [12]. Such a method relies on the equivalent age concept, whose definition is derived from Arrhenius' Law:

$$t_{eq} = \int_0^t \exp\left(-\frac{E_a}{R}\left(\frac{1}{T(\tau)} - \frac{1}{T_{réf}}\right)\right)d\tau \tag{15}$$

Provided preliminary calibration has been carried out, a simple measurement of the *in situ* concrete temperature change then makes it possible to deduce the material's compressive strength. Such a calibration step for this method entails determining:

– the evolution in compressive strength vs. equivalent age at the reference temperature (typically 20°C, i.e. 293 Kelvin);
– apparent activation energy E_a.

Maturity measurements are often presented as a method to be implemented onsite for generating early-age predictions of how a set concrete will evolve mechanically. While associated with numerical tools, these measurements also offer other advantages. As indicated above, the TEXO module of the CESAR-LCPC computation code simulates temperature fields inside a given structure. Applying a maturity evaluation based on thermal simulation results (note: temperature evolution is not measured but rather simulated) leads to concrete strength capacities at any point of the structure and at any point in time. These capacities, expressed in terms of compressive strength, can be compared with the early-age mechanical requirements contained in the set of design specifications.

Depending on the expected outcome, it is entirely possible to modify the selected concrete formula, the formwork removal schedule or concreting phasing, in addition to proposing a heat curing treatment. The ensuing results and choices derived from this preliminary study obviously depend on the relevance of the models introduced and input material data, as well as the simplifying hypotheses adopted during the modeling stage. Such hypotheses are nonetheless quite helpful when preparing

sites with perceived complex construction conditions; they allow limiting the number of tests to be performed during the design phase and planning for the actual construction phase with greater reassurance.

TEXO-MEXO: A SIMPLE TOOL FOR ANALYZING CRACKING RISKS

The benefit of linking these two CESAR-LCPC modules is to offer the professional a simple tool for analyzing cracking risks during the early age of concrete structures. The term "simple tool" used here should not be confused with "simplistic tool", since its output simulations are already sufficiently refined to envisage the three-dimensional complexity of the structures being depicted.

The focus however remains on merely indicating a cracking "risk", given that the mechanical computations are still based on an elastic estimation of stress states. This risk is therefore estimated from an initial cracking criterion, which could for example be expressed by comparing the major principal stress with a tensile strength value for the material at an age corresponding to time t of the computation. This strength may in turn be directly determined as a function of degree of hydration, hence of r, at the same age by assuming a linear relationship between the two parameters, along the lines of what was proposed in Equation **(12)** for compressive strength. Since these computations lie within the linear domain, without any recall of cracking history, they may lead to an overestimation of the actual stress state (i.e. absence of stress relaxation due to cracking, no inclusion of delayed effects) and thus to an actual of risk of cracking.

Comparing zones subjected to the highest tensile stresses with a cracking face obtained *in situ* is theoretically impossible since the mechanical model does not take cracking mechanisms into account. Modeling results can however yield an initial approach to locating high-risk zones in addition to identifying (or discerning) a set of technical solutions.

CASE STUDY

■ Presentation of the case study and its context

While the influence of early-age concrete behavior is in many cases relegated to simple approaches, for some of the more complex structures or those containing massive or slender elements, it proves necessary to grasp the impact of this phenomenon, prior to the execution phase, so as to minimize the risk of early-age cracking.

Figure 1
Overview of the breakwater under construction

Figure 2
Top view of a box girder during building of the superstructure shear walls

For this last reason, a specific approach was implemented as part of a box girder superstructure project, with this element constituting the main component of the breakwater at the "roll-on, roll-off" (RORO) port in Tangier, Morocco (see **Figs. 1** and **2)**.

1 | 2

The superstructure shear walls were mainly cast in place following the launch and positioning of the lower part of the box girder assembly. Prefabricated using a sliding formwork, these walls feature a curved geometry and contain a panel joint capable of withstanding a stress concentration during the concrete cooling phases following setting.

The purpose of the study undertaken consisted of examining various construction phasing solutions in order to determine the one that would minimize the risk of generating residual tensile stresses capable of inducing permanent cracking.

■ Computation method and model

For this study, a three-dimensional model was developed using the CLEO software package (which is the new CESAR-LCPC interface). At first, a thermal computation was performed with the TEXO module; the result provided the temperature field $T(t)$ along with the level of concrete hydration progress $r(t)$. These data were then used as input into a mechanical model, which through an elastic computation (namely via the MEXO module) yields the structure's stress field a function of mechanical properties calculated at each time step with respect to fields $T(t)$ and $r(t)$ ($E(r)…$).
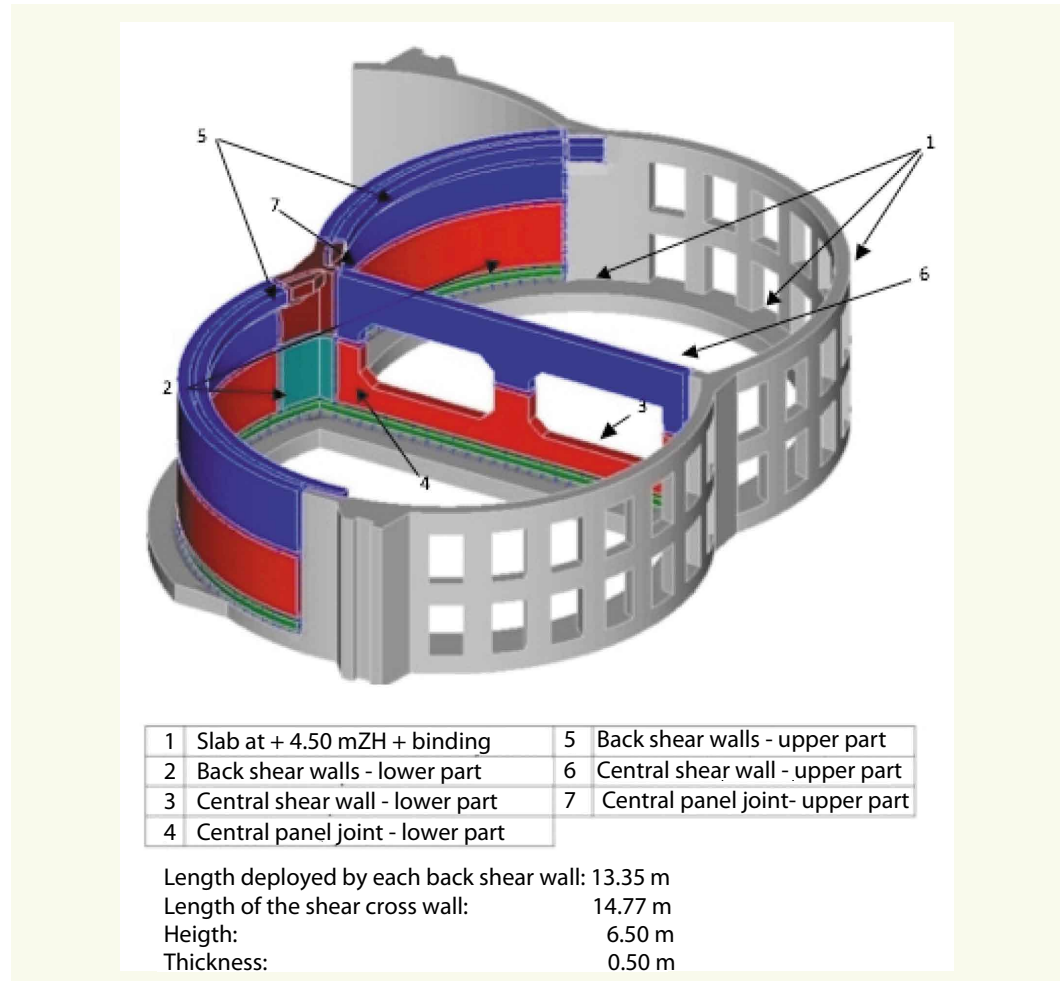
Figure 3 illustrates this computation model in addition to describing shear wall geometry.

■ Construction phasing sequences under study

The model has been designed to allow evaluating 4 different types of phasing for casting the project's shear walls; these configurations are as follows:

– Configuration M1: Set of studs 2 through 7 cast simultaneously

Figure 3
Computation model geometry

1	Slab at + 4.50 mZH + binding	5	Back shear walls - upper part
2	Back shear walls - lower part	6	Central shear wall - upper part
3	Central shear wall - lower part	7	Central panel joint- upper part
4	Central panel joint - lower part		

Length deployed by each back shear wall: 13.35 m
Length of the shear cross wall: 14.77 m
Heigth: 6.50 m
Thickness: 0.50 m

– Configuration M2: 1st embankment studs 2, 3, 5, 6; 2nd studs 4, 7
– Configuration R1: 1st embankment studs 2, 3; 2nd studs 5, 6; 3rd studs 4, 7
– Configuration R2: 1st embankment studs 2, 4; 2nd studs 5, 6, 7.

In all cases, the structural elements already built (slab at +4.50 plus shear walls, shown with gray shading in **Fig. 3**) are considered to be completely hardened (beyond an age of 28 days) at the time of casting studs 2 through 7. Moreover, since shear wall reinforcement **(Fig. 4)** had been laid out prior to concreting, all computations are assumed to be offset temporally by 48 hours between the casting of 2 consecutive embankments.

Figure 4
Detailed view of the central shear wall and panel joint between the curved shear walls
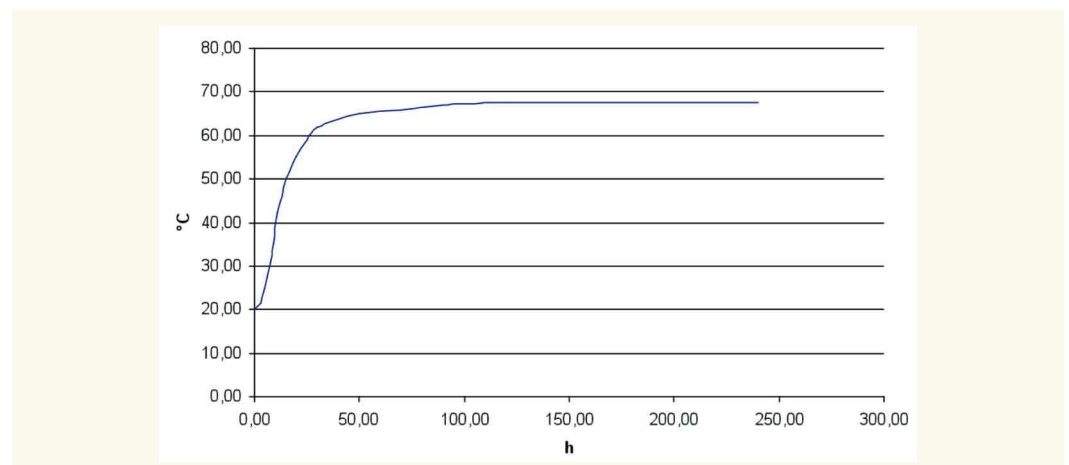

■ Input data for thermal computations

› Concrete

For the concrete specimen, the main characteristics used are as follows:

– Type of concrete: C50
– Young's modulus: E = 40,520 MPa
– Coefficient of thermal expansion: $\alpha = 10^{-5}\,K^{-1}$
– Final endogenous shrinkage: $\varepsilon_f = 8.4\ 10^{-5}$
– Q_{AB} **curve: see Fig. 5**
– Heat capacity: C = 666.7 Wh/m^3/K
– Conductivity: K = 1.67 W/m/K

The concrete is cast at an initial temperature of 20°C within an environment where the outside temperature is assumed to be constant over the study period and equal to 25°C.

Figure 5
Corrected Q_{AB} curve

The coefficients of heat exchange between the concrete and the external medium are equal to:

– Casting using form panels or in open air: $\lambda = 6$ W/m²/°C

– Exchanges on elements other than shear walls: $\lambda = 3$ W/m²/°C.

For this model, the mechanical boundary conditions introduced correspond to a locking of the slab on which the studied shear walls were cast.
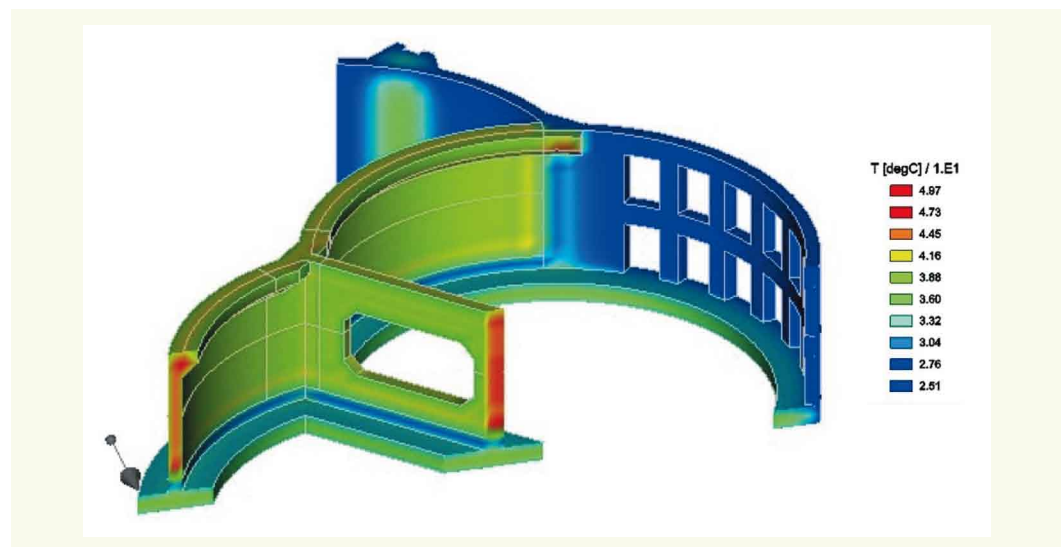
■ Results

› Temperature

As anticipated, the analysis of these results has focused, for each computation, on the temperature rises and gradients between the various elements along with their comparison.

Figure 6 provides a sample graphical output generated using the software, revealing at a given point in time the temperature iso-value zones within structural elements; a cross-sectional cut of this output demonstrates (in Fig. 6 below) the temperature profile at the shear wall core.

Figure 6
Temperature iso-values

Interpretation of these results on a 3D model proves to be slightly more complex than for a plane model and involves studying temperature variations over time for groups of points or cross-sections, which have been carefully identified and selected from outputs of the same type as that presented above.

› Strains - Stresses

Similarly, for each time step, the various principal stresses and strains can be visualized and analyzed.

Figure 7 indicates, at a given time *t* for the M1 phasing, the deformed geometry of the structure along with the displacement values (shown here in the u direction parallel to the central shear wall).

Figure 8 displays, at the very same time, the iso-values of tensile stresses, under the same conditions (M1 phasing), responsible for yielding the highest results.

› Cracking risk

The principle behind this assessment of concrete cracking likelihood is based on a comparison of tensile stress in an element, as provided by computation, with its estimated strength at the same age (i.e. approx. 10% of its compressive strength).
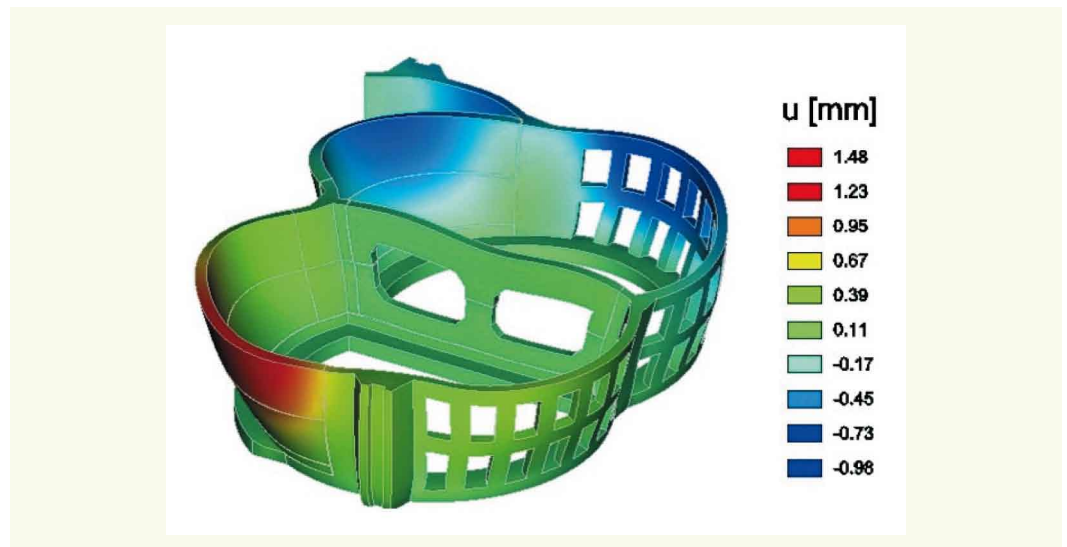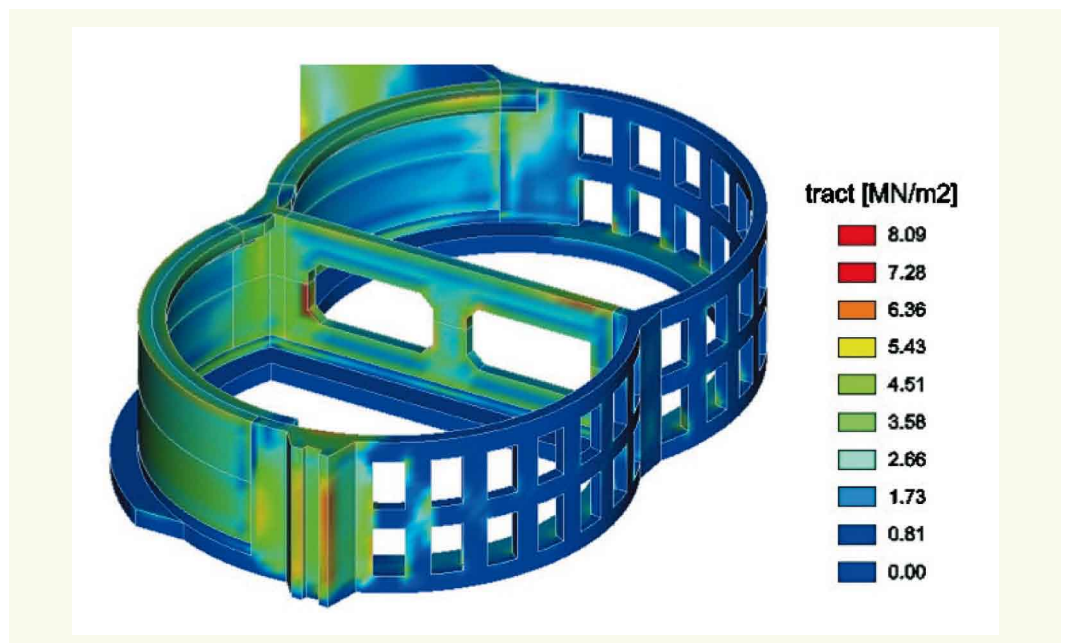
Given that the constitutive law used for this concrete specimen is elastic, then such an approach proves rather conservative, to the extent that the model does not incorporate an eventual redistribution of stresses after cracking.

Feedback reveals that some flexibility can be allowed when estimating this strength with respect to the type of cracking taken into account for the targeted structure.

■ Conclusion of this study

Comparing results among the various foreseen scenarios underscores both the need to install the central panel joint as a follow-up step, so as to avoid generating excessive tensile stresses at the shear wall interface, and the negligible influence of shear wall casting height (on 1 or 2 embankments). Moreover, the M2 phasing solution was suggested given its associated very low risk of cracking during the early age despite having cast the shear walls over the entire height using just a single phase.

OVERALL CONCLUSION

This document offers a concise presentation of the simple simulation tools available for studying the thermomechanical behavior of concrete at an early age and for analyzing cracking risks. These tools make it possible to perform studies preliminary to the actual construction, thus optimizing: the choice of concrete mix design, concreting phasing, and the eventual introduction of a special treatment (e.g. heat curing). The experiments and experience relative to actual use examples indicate the capacity of such tools in yielding pertinent results, especially in the case of massive structures.

Their apparent simplicity however should not overshadow the fact that these tools cannot be expected to offer comprehensive predictions. The underlying hypotheses are not sufficiently refined to reliably predict, for example, an actual state of cracking or damage on the structural skin. This caveat is a critical one in the case of a structural durability study in particular, e.g. when estimating reinforcement corrosion risks. A considerable amount of research is currently being devoted to this point, with LCPC leading the way.

REFERENCES

1 HUMBERT P., CESAR-LCPC : un code général de calcul par éléments finis. *Bulletin de Liaison des Laboratoires des Ponts et Chaussées*, n° 160, pp. 112-115, mars-avril,**1989**.

2 Logiciels LPC : CESAR-LCPC, Laboratoire Central des Ponts et Chaussées, ISBN 2-7208-8520-0, pp. 58-65, **1994**.

3 LE CHATELIER H., Sur les changements de volume qui accompagnent le durcissement des ciments, *Bull. de la société pour l'Encouragement de l'Industrie Nationale*, Paris, 5e série, vol 5, pp. 54-57, **1900**.

4 BYFORS J., Plain concrete at early ages, *CBI Research* N°3 :80, 464 p., Swedish Cement and Concrete Research Institute, Stockholm, Sweden, **1980**.

5 ULM F.-J., COUSSY O., Modelling of Thermo-mechanical Couplings of Concrete at Early Ages, *Journ. of Eng. Mech.*, July, pp. 785-794, **1995**.

6 POWERS G., BROWNYARD T. L., Studies of the physical properties of hardened Portland cement paste, *Res. Bull.* 22, Portland Cement Association, Skokie, **1948**.

7 ULM F.-J., COUSSY O., What is a "massive" concrete structure at early ages? Some dimensional arguments, *Journ. of Eng. Mech.*, May, pp. 512-522, **2001**.

8 BENBOUDJEMA F., TORRENTI J.-M., Early age behaviour of concrete nuclear containments, *Nuclear Eng. And Design*, 238, pp. 2495-2506, **2008**.

9 ACKER P., TORRENTI J.-M., ULM F.-J., eds, *Comportement du béton au jeune âge*, Hermès-Lavoisier, ISBN 2-7462-0985-3, **2004**.

10 GLUAIS A., *Essais quasi adiabatiques sur bétons (QAB)*, projet de mode opératoire FAER n° 1.30.12.3 du 14 mars **1985**.

11 ALEGRE H., La calorimétrie des Ciments au CERILH, *Publication Technique* n° 119, CERILH, **1961**.

12 Résistance du béton dans l'ouvrage – La maturométrie, *Coll. Techniques et Méthodes des Laboratoires des Ponts et Chaussées*, Guide Technique, LCPC, ISSN 1151-1516, 66 p., mars, **2003**.

13 BOULAY C., TORRENTI J.M., ANDRÉ J.L., SAINTILAN R., Essais avec le calorimètre quasi adiabatique pour bétons, *BLPC*, n° 278, **2010**, pp. 19-36.